university of groningen

University Medical Center Groningen

University of Groningen

Probing and Tuning the Spin Textures of the K and Q Valleys in Few-Layer MoS2

Chen, Qihong; El Yumin, Abdurrahman Ali; Zheliuk, Oleksandr; Wan, Puhua; Liang, Minpeng; Peng, Xiaoli; Ye, Jianting

Published in:
Physica status solidi-Rapid research letters

DOI:
10.1002/pssr.201900333

IMPORTANT NOTE: You are advised to consult the publisher's version (publisher's PDF) if you wish to cite from it. Please check the document version below.

Document Version
Publisher's PDF, also known as Version of record

Publication date:
2019

Link to publication in University of Groningen/UMCG research database

Citation for published version (APA):
Chen, Q., El Yumin, A. A., Zheliuk, O., Wan, P., Liang, M., Peng, X., & Ye, J. (2019). Probing and Tuning the Spin Textures of the K and Q Valleys in Few-Layer MoS2. *Physica status solidi-Rapid research letters*, *13*(12), [1900333]. https://doi.org/10.1002/pssr.201900333

Copyright
Other than for strictly personal use, it is not permitted to download or to forward/distribute the text or part of it without the consent of the author(s) and/or copyright holder(s), unless the work is under an open content license (like Creative Commons).

The publication may also be distributed here under the terms of Article 25fa of the Dutch Copyright Act, indicated by the “Taverne” license. More information can be found on the University of Groningen website: https://www.rug.nl/library/open-access/self-archiving-pure/taverne-amendment.

Take-down policy
If you believe that this document breaches copyright please contact us providing details, and we will remove access to the work immediately and investigate your claim.

Downloaded from the University of Groningen/UMCG research database (Pure): http://www.rug.nl/research/portal. For technical reasons the number of authors shown on this cover page is limited to 10 maximum.

Download date: 05-06-2022

physica status solidi rrl
www.pss-rapid.com

Check for updates

Probing and Tuning the Spin Textures of the K and Q Valleys in Few-Layer MoS_2

*Qihong Chen, Abdurrahman Ali El Yumin, Oleksandr Zheliuk, Puhua Wan, Minpeng Liang, Xiaoli Peng, and Jianting Ye**

The strong spin–orbit coupling along with broken inversion symmetry in transition metal dichalcogenides (TMDs) results in spin polarized valleys, which are the origins of many interesting properties such as Ising superconductivity, circular dichroism, valley Hall effect, etc. Herein, it is shown that encapsulating few-layer MoS_2 between hexagonal boron nitride (h-BN) and gating the electrical contacts by ionic liquid pronounce Shubnikov–de Haas (SdH) oscillations in magnetoresistance. Notably, the SdH oscillations remain unchanged in tilted magnetic fields, demonstrating that the spins of the Q/Q' valleys are firmly locked to the out-of-plane direction; therefore, Zeeman energy is insensitive to the in-plane magnetic field. Ionic liquid gating induces superconductivity on the surface of unencapsulated MoS_2. The spins of Cooper pairs are strongly pinned to the out-of-plane direction by the effective Zeeman field, hence are protected from being realigned by an in-plane magnetic field, namely, Ising protection. As a result, superconductivity persists in an in-plane magnetic field up to 14 T, in which T_c only decreases by ≈0.3 K from T_{c0} as ≈7 K. By applying back gate, the strength of Ising protection can be effectively tuned, where an increase in 70% is observed when back gate changes from +90 to −90 V.

The concept of spin- and valley-tronics is to use the spin and valley degrees of freedom to store and manipulate information.[1,2] Transition metal dichalcogenides (TMDs) such as MoS_2, WS_2, WSe_2, etc. are layered 2D semiconductors with band extrema at the K and Q (about half way between Γ and K of the first Brillouin zone) points.[3] The band structure is thickness dependent, meaning that the lowest energy of the conduction band resides at the K and Q valleys for monolayer and multilayer TMDs, respectively. Because of the strong spin–orbit coupling (SOC) and broken inversion symmetry caused by either isolating a monolayer or field-effect gating, the spin degeneracy is lifted and the polarization is locked to the out-of-plane direction, alternating for adjacent layers. The coupled spin and valley degrees of freedom make TMDs an ideal playground to explore applications in spin- and valleytronics. The spin texture at the K/K' valleys of the valence and conduction band has been widely studied by optical measurements, thanks to the direct bandgap nature that enhances optical transition;[4,5] whereas the transition from the K/K' point of the valence band to the Q/Q' point of the conduction band is indirect, which gives a much weaker contribution to the optical response. In contrast, quantum oscillations in magnetoresistance (MR) have been proved to be a useful tool to study the electronic properties of the conduction band extrema of both K and Q pockets.[6–10] Nevertheless, the observation of quantum oscillations requires not only high carrier mobility but also high-quality electrical contact. The mobility can be significantly improved by encapsulating TMDs between hexagonal boron nitride (h-BN) flakes, which serves as an atomically flat substrate and isolates charged impurity scatterings commonly found in the SiO_2 substrate. Different approaches have been proposed to enhance the electrical contact with TMDs such as by using graphene as a contacting electrode[11] and selective etching,[12] yet more efficient ways to generate high-quality electrical contacts are still being intensively explored.

In this study, we show that high-quality electrical contact can be achieved in a simple and effective way—using ionic liquid gating between normal electrodes and TMDs. Ionic liquid gating works similar to a traditional field-effect transistor (FET), except that ionic liquid is used as the gating media to replace the traditional oxide. A gate bias drives the ions to the channel surface and induces carriers with density up to the range of $\approx 10^{14}$ cm^{-2}. In this high carrier density regime, semiconducting TMDs, e.g., MoS_2,[13] $MoSe_2$,[14] and WS_2,[15,16] are turned into superconductors. Here, we focus on few-layer MoS_2, where both Q/Q' and K/K' valleys can be accessed by field-effect doping. By encapsulating MoS_2 with h-BN, well-defined Shubnikov-de Haas (SdH) oscillations are observed in the magnetotransport measurement. The effective mass extracted from the temperature dependence of the oscillation amplitude is 0.6 m_e, in good agreement with theoretical calculations. The observed Landau-level degeneracy $g = 3$ confirms that the conducting electrons are contributed by the Q/Q' valleys of the conduction band, where the degeneracy between the 3 Q and 3 Q' valleys in the first Brillouin zone is

Dr. Q. Chen, A. Ali El Yumin, O. Zheliuk, P. Wan, M. Liang, X. Peng, Prof. J. Ye
Device Physics of Complex Materials
Zernike Institute for Advanced Materials
University of Groningen
Nijenborgh 4, Groningen 9747 AG, The Netherlands
E-mail: j.ye@rug.nl

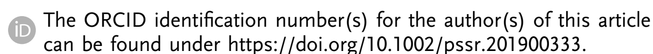
The ORCID identification number(s) for the author(s) of this article can be found under https://doi.org/10.1002/pssr.201900333.

DOI: 10.1002/pssr.201900333

 © 2019 WILEY-VCH Verlag GmbH & Co. KGaA, Weinheim

lifted by the valley's Zeeman effect in the presence of an external field. The SdH oscillations remain unchanged in a tilted magnetic field up to 46.5°, indicating that the spins of the Q/Q' valleys are strongly locked to the out-of-plane direction; hence, Zeeman energy is not sensitive to the in-plane field component. In addition to the SdH oscillations in the Q/Q' valleys, superconductivity is induced at the surface of unencapsulated MoS_2, where Cooper pairs reside at the K/K' valleys of the conduction band. Strong SOC in TMDs and inversion symmetry breaking (by the electrical field of ionic gating) induce a Zeeman-like effective magnetic field B_{eff} (≈100 T), which locks the spins of electrons to the out-of-plane directions; thus, the spins of Cooper pairs are protected from being realigned by an in-plane magnetic field, namely, Ising protection. As a result, while superconductivity is completely suppressed by applying moderate out-of-plane magnetic fields, the transition temperature only decreases by ≈0.3 K in an in-plane field of 14 T. Furthermore, the strength of Ising protection can be effectively tuned by the back gate. The in-plane upper critical field shows an increase in 70% at $V_{BG} = -90$ V compared with $V_{BG} = 90$ V at $B = 14$ T. While this behavior is not well understood yet, a possible explanation may be that the interlayer coupling increases with increasing V_{BG}, leading to the decrease in Zeeman effective field; hence, the pinning effect weakens.

To achieve high mobility and high-quality electrical contact, we fabricated van der Waals heterostructures where MoS_2 is sandwiched between two h-BN flakes with a partially exposed MoS_2 surface for electrical contact. Few-layer MoS_2 and h-BN were separately prepared by the mechanical exfoliating of bulk single crystals on silicon wafers covered with 300 nm SiO_2. Following the well-known dry transfer technique,[17] we transferred a selected MoS_2 flake onto a thin (≈30 nm) and uniform h-BN flake, which serves as the direct contacting substrate. Another carefully chosen h-BN flake with a nearly rectangular shape was transferred to partially encapsulate the MoS_2 flake, as schematically shown in **Figure 1**a. The electrodes composed of Ti/Au (5 nm/50 nm) were patterned with standard e-beam lithography. A large gold pad was designed close to the device for applying liquid gate bias. A small droplet of ionic liquid (*N*,*N*-diethy-*N*-2-methoxyethyl)-*N*-methylammonium bis-(trifluoromethylsulfonyl)-imide (DEME-TFSI) was applied to cover both the device and gold pad. Afterward, the whole device was

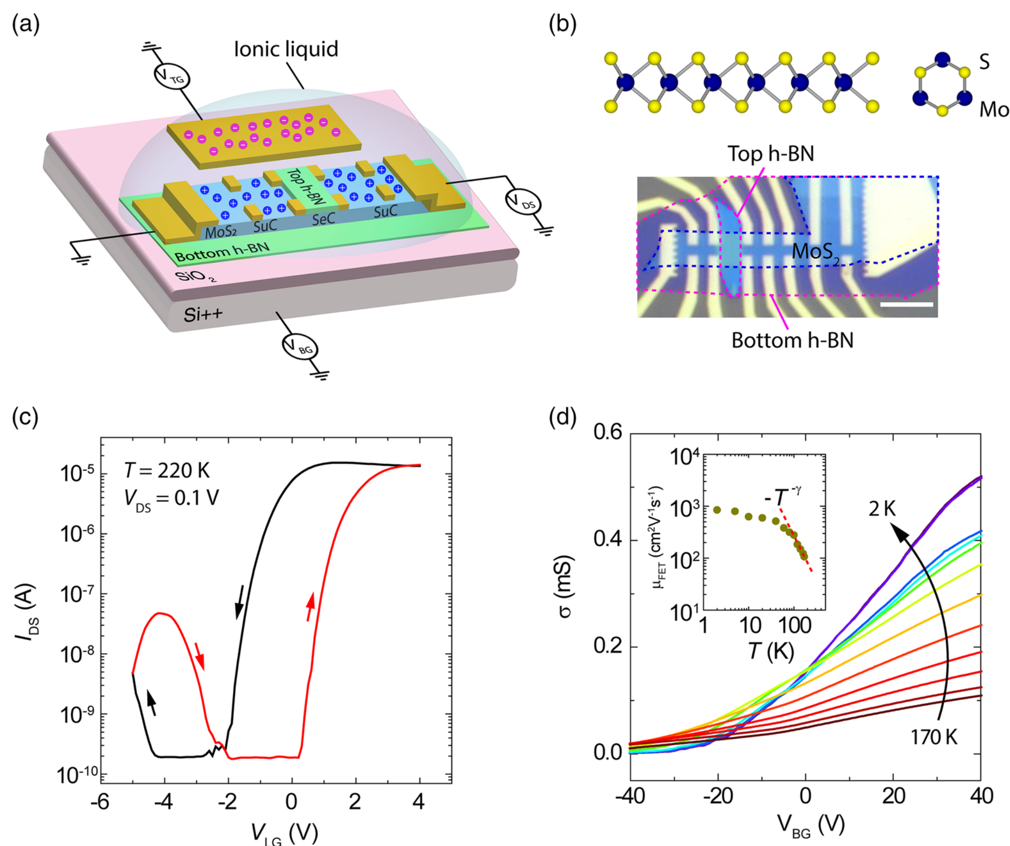

Figure 1. Device characterization. a) Schematic illustration of the device configuration. An h-BN flake with proper size partially encapsulates MoS_2. This area remains intrinsically semiconducting, whereas the unencapsulated surface becomes superconducting and good electrical contacts are made in this area. "SuC" and "SeC" are short for superconducting and semiconducting, respectively. b) Up: Crystal structure of a monolayer MoS_2 from the side and top view. Bottom: Optical image of a typical device. The MoS_2 and h-BN flakes are outlined by blue and purple dashed lines, respectively. The scale bar is 5 μm. c) Transfer curve by ionic gating at $T = 220$ K, with $V_{DS} = 0.1$ V. The color-matched arrows indicate the scan direction. d) Four-probe sheet conductivity as a function of V_{BG} at different temperatures from 170 to 2 K. Inset: FET mobility obtained by fitting the transfer curve with back gate capacitance $\mu_{FET} = \frac{1}{C_g}\frac{d\sigma}{dV_g}$. The red dashed line shows the power law relation $\mu(T) \sim T^{-\gamma}$, with $\gamma = 1.73$.

© 2019 WILEY-VCH Verlag GmbH & Co. KGaA, Weinheim

loaded to a cryostat equipped with a superconducting magnet from Cryogenic UK. Transport measurements were performed using the standard lock-in amplifiers (Stanford Research SR830). Liquid gate and back gate voltages were set by a direct current (DC) source meter (Keithley 2450).

Figure 1b shows the crystal structure of MoS_2 and the optical image of a typical device, respectively. The unencapsulated MoS_2 surface is in contact with the ionic liquid; therefore, metallic electrical contact that is even superconducting can be easily achieved in this area through ionic gating. The transfer curve for the unencapsulated area by ionic gating is shown in Figure 1c, where the arrows indicate the scan direction of gate voltage. Ionic gating was performed at $T = 220$ K, where the ions are still moveable, yet electrochemical reaction is suppressed as reported previously.[13,16,18–21] The device can be easily switched on and off by applying small ionic gate voltage. Both electron and hole conduction can be induced, showing an ambipolar transistor operation with a current on/off ratio higher than 10^5 in the dominating electron side. Hysteresis is observed due to low ionic mobility near the glass transition temperature, namely, the ion movements are relatively slow at this low temperature. With ionic gate voltage fixed, the device is cooled down below $T = 180$ K, where the ionic liquid is frozen; hence, gate voltage can be retracted without losing gating effect.

For the h-BN-encapsulated area, ionic liquid is separated from the MoS_2 surface. This area remains almost unaffected by ionic gating, showing intrinsic semiconducting properties of few-layer MoS_2. Figure 1d shows the transfer curve by back gate (V_{BG}) for the h-BN-encapsulated area at different temperatures. For $V_{BG} > 0$ V, the device shows metallic behavior as the conductivity increases with decreasing temperature. Electron mobility can be extracted from the gate dependence of sheet conductivity by $\mu_{FET} = (1/C_g)(d\sigma/dV_g)$, where σ is the sheet conductivity and $C_g = 10.5\text{nF}/\text{cm}^{-2}$, which is the capacitance per unit area for the back gate of 300 nm SiO_2 and 30 nm h-BN used in this experiment. The extracted FET mobilities at different temperatures are shown in the inset of Figure 1d. At $T = 170$ K, $\mu_{FET} \sim 100\,\text{cm}^2/\text{Vs}^{-1}\text{Vs}$, which increases with decreasing temperature, with a tendency to saturate below $T = 80$ K. At $T = 2$ K, $\mu_{FET} \sim 1000\,\text{cm}^2/\text{Vs}^{-1}\text{Vs}$, showing almost one order of magnitude improvement. The measured mobility can be described by a simple formula: $1/\mu(T) = 1/\mu_{imp} + 1/\mu_{ph}(\text{T})$, where $\mu_{imp}(T)$ is the contribution from impurity scattering and $\mu_{ph}(T)$ is the temperature-dependent contribution from phonon scattering.[11] At high temperatures, phonon scattering is the main source that limits the mobility of electrons. The temperature dependence of $\mu_{ph}(T)$ is described by the power law $\mu_{ph}(T) \sim T^{-\gamma}$. The best fitting of our data gives an exponent of $\gamma = 1.73$, which is within the range of the previously reported values 1.9–2.5[11,12] and 0.55–1.7.[22,23] At sufficiently low temperatures, the phonon scatterings are completely suppressed and the main scattering sources are from long-range coulomb impurities and short-range atomic defects.[24–26] As these scatterings have a very weak temperature dependence, mobility saturates at a low temperature.

The MR curves for different V_{BG} are shown in **Figure 2**a for the encapsulated MoS_2, where clear Shubnikov-de Haas (SdH) oscillations appear at $B > 5$ T. To extract the oscillation components, we take the average of the top and bottom envelope lines (determined by the peaks and valleys of the oscillations) as the MR background. After subtracting the MR background, the oscillations shown in Figure 2b are periodic functions of $1/B$, in which the amplitude and period of the SdH oscillations change with the increase in V_{BG}. In 2D electron gas (2DEG), the carrier density is directly related to the period of quantum oscillations through $n_{2D} = geB_F/h$, where the Landau-level degeneracy $g = g_s \cdot g_v$ is the product of the spin and valley degeneracies and B_F is the oscillation frequency in $1/B$, which can be obtained from Figure 2b. In contrast, carriers induced by back gate can be calculated through geometric capacitance and gate voltage, $n_{2D} = C_g(V_{BG} - V_{th})/e$. Here, V_{th} is the threshold voltage and $C_g = 10.5\,\text{nF}/\text{cm}^{-2}$. Hence $B_F = (hC_g/ge^2)(V_{BG} - V_{th})$, the Landau-level degeneracy g can be obtained from the linear fitting of back gate dependence of B_F. In Figure 2c, the fitting result $g = 3.06$ is in good agreement with that reported in the literature.[6,12,27] The threefold Landau level suggests that the conducting electrons are from the Q/Q' valleys as there are 3 Q and 3 Q' valleys in the first Brillouin zone, and the degeneracy between Q and Q' valleys is lifted at a high field due to the valley Zeeman effect (right panel of Figure 2c),[28–31] leading to a degeneracy of 3.

According to the Lifshitz–Kosevich formula, the oscillation amplitude at a fixed magnetic field is described by $\Delta R \propto \alpha T/\sinh(\alpha T)$, where $\alpha = 2\pi^2 k_B/\hbar\omega_c$, and $\omega_c = eB_\perp/m^*$ is the cyclotron frequency with m^* being the effective mass. Therefore, m^* can be determined by fitting the temperature-dependent oscillation amplitudes with this formula (Figure 2d). As shown in Figure 2e, for $V_{BG} = 100$ V, the best fitting yields an effective mass of $m^* = 0.6m_e$ at $B = 9.4$ T, where m_e is bare electron mass. Fittings at other magnetic fields give very similar values (Figure 2f). This result matches well with the theoretical calculation of the MoS_2 band structure,[32] which predicts that there are two bands near the Fermi level (K and Q valleys), with the lowest energy of the conduction band at the K/K' valleys ($m^* = 0.5m_e$) for monolayer, and the Q/Q' valleys ($m^* = 0.6m_e$) become the lowest of the conduction band for multilayer.

For 2DEG, the Landau levels are equally spaced by the cyclotron energy, $E_c = \hbar\omega_c = \hbar eB_\perp/m^*$, which is determined by the out-of-plane component of the magnetic field $B_\perp$. In contrast, Zeeman energy is proportional to the total magnetic field, $E_Z = g^*\mu_B B_t$, where g^* is the effective g factor, μ_B the Bohr magneton, and B_t the total magnetic field. Therefore, the Zeeman-to-cyclotron energy ratio is given as $E_Z/E_c = g^*\mu_B B_t m^*/\hbar eB_\perp \propto 1/\cos(\theta)$. Here, $\cos(\theta) = B_\perp/B_t$ with θ defined as the angle between magnetic field and the normal of the 2D plane (inset of Figure 2g). The value of $\cos(\theta)$ determines the Landau-level filling sequence. In our measurement, we see that the oscillations remain unchanged for different tilting angles up to 46.5°, as shown in Figure 2g. This observation suggests that even for multilayer MoS_2, the spins of the Q/Q' valleys are strongly locked to the out-of-plane direction; hence, Zeeman energy is insensitive to the in-plane magnetic field component.

Next, we focused on the superconductivity in the unencapsulated area. When the carrier density induced by ionic gating reaches the level of $\approx 10^{14}\,\text{cm}^{-2}$, MoS_2 becomes superconducting with transition temperature $T_c \approx 7$ K. Here, T_c is defined as the temperature where the resistance is half of the normal-state resistance. As shown in **Figure 3**a, superconductivity gradually

© 2019 WILEY-VCH Verlag GmbH & Co. KGaA, Weinheim

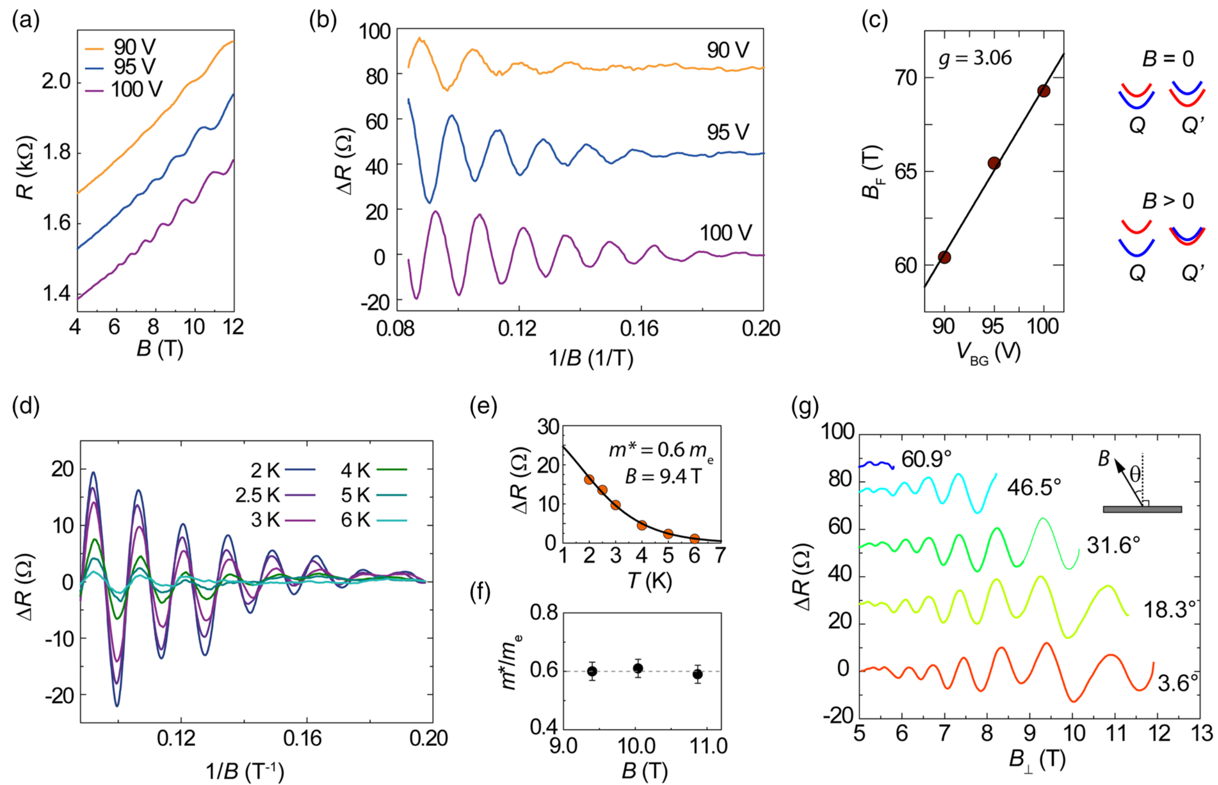

Figure 2. Quantum oscillations in the encapsulated area. a) Magnetoresistance (MR) measured at $T = 2$ K for $V_{BG} = 90$, 95, and 100 V from top to bottom, respectively. b) ΔR as a function of $1/B$ after subtracting the MR background. Curves are vertically shifted by 40 Ω for clarity. c) Left: Oscillation period B_F as a function of V_{BG} obtained from panel (b). With $B_F = (hC_g/ge^2)(V_{BG} - V_{th})$, the linear fitting yields a Landau-level degeneracy of $g = 3.06$. Right: Spin diagrams of the Q/Q' valleys, showing valley degeneracy at zero field and the valley Zeeman splitting at a high field. Red and blue colors represent up and down spin polarization, respectively. d) Quantum oscillations at different temperatures for $V_{BG} = 100$ V. e) Temperature dependence of the oscillation amplitude at $B = 9.4$ T. Solid line is the best fitting using the Lifshitz–Kosevich formula, yielding an electron effective mass of 0.6 m_e. f) Effective mass from fittings at different magnetic fields. g) The SdH oscillations as a function of $B_\perp$ at different titled angles. The curves are vertically shifted for clarity. Inset: Schematic illustration of the tilting angle between the field and sample.

weakens by applying an out-of-plane magnetic field and gets completely suppressed at $B = 14$ T. In sharp contrast, applying an in-plane field of $B = 14$ T has very little effect on superconductivity. As shown in Figure 3b, T_c only decreases by ≈0.3 K compared with zero field. Due to the strong screening effect, the induced carriers are mainly confined at the K/K' valleys of the topmost layer. Strong spin-orbit interaction and inversion symmetry breaking induce a Zeeman-like effective magnetic field B_{eff}, pointing to the out-of-plane direction (Figure 3d). The magnitude of this B_{eff} is in the order of ≈100 T, therefore strongly pins the spins of the K/K' valley electrons to the out-of-plane direction. This is compatible with the spin configuration of Cooper pairs as the spin polarizations are opposite at the K and K' valleys. As a result, the spins are not easily realigned by an in-plane magnetic field; thus, superconductivity is protected, which is known as Ising protection.

Surprisingly, the strength of Ising protection can be effectively tuned by applying V_{BG} through 300 nm SiO_2. Figure 3c shows the parallel upper critical field as a function of reduced temperature. Here, the upper critical field is normalized by the Pauli paramagnetic limit, $B_p = 1.86\, T_{c0}$, which describes the upper limit of critical field due to the competition between Zeeman splitting energy and the binding energy of Cooper pairs. The T_{c0} here is the zero-field superconducting transition temperature. As shown in Figure 3c, with Ising protection, the in-plane upper critical field can easily break the Pauli limit. As V_{BG} decreases from 90 to −90 V, Ising protection becomes stronger, manifesting as an upward shift of the B_{c2}–T_c curve. At small or negative V_{BG}, there is "a vertical region" (a light purple line in Figure 3c) where T_c remains unchanged at low magnetic fields. As the field further increases, T_c starts to decrease, showing a quasi-linear relation between T_c and B_{c2} up to our measured field range. The inset of Figure 3c shows the slope of the best linear fitting, which exhibits a monotonic behavior as a function of V_{BG}, i.e., the slope deceases with increasing V_{BG}. A larger slope leads to a higher upper critical field at zero temperature, suggesting stronger Ising protection. This tuning effect is not understood well yet, and the following section provides a possible explanation.

It is well known that although ionic gating induces a large density of carriers, the carrier concentration decays exponentially from the top to bottom due to the strong Thomas–Fermi screening effect. The amount of carriers in the second layer is only 10% of that in the topmost layer. Due to this strong confinement, superconductivity resides exclusively in the topmost layer,

 © 2019 WILEY-VCH Verlag GmbH & Co. KGaA, Weinheim

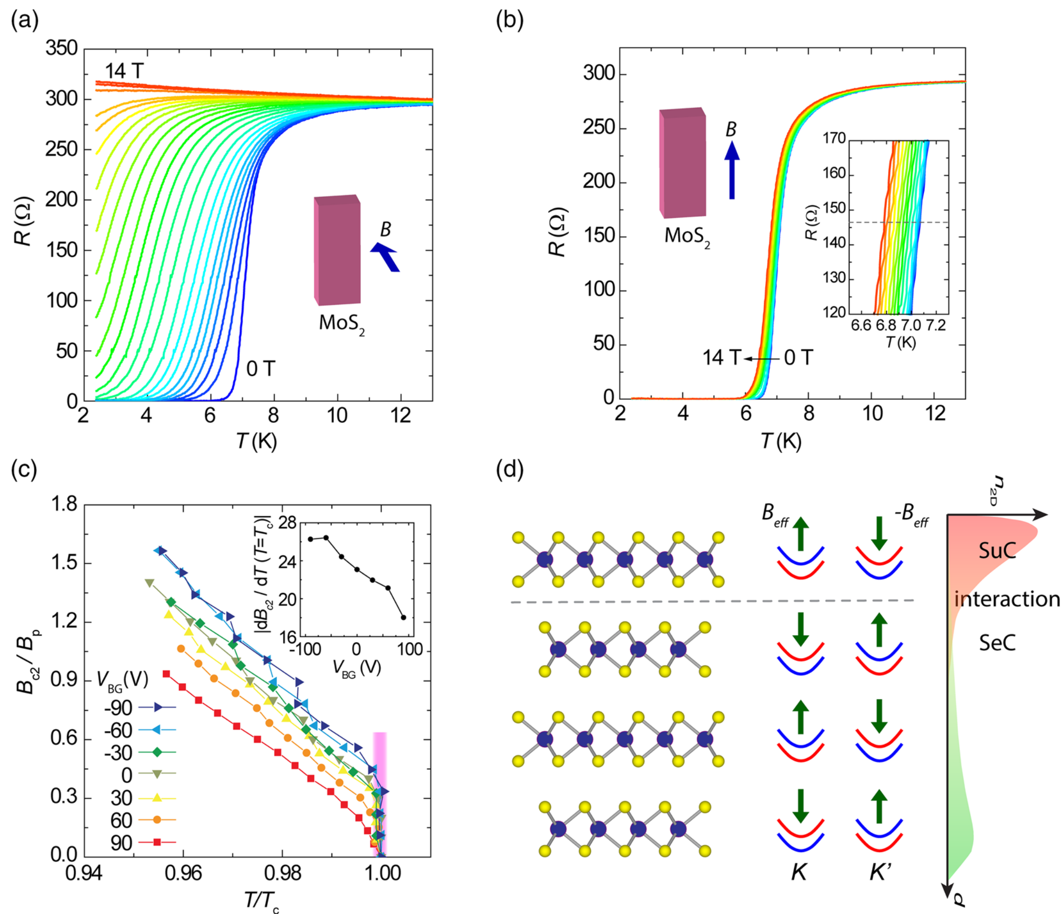

Figure 3. Superconductivity in the unencapsulated area. a) Temperature dependence of resistance under different perpendicular magnetic fields, from 0 to 1 T in 0.2 T steps, 1, 1.3, 1.6 T, 2 to 8 T in 0.5 T steps, and 8 to 14 T in 2 T steps. Inset: Schematic illustration of the applied magnetic field and MoS_2 plane. b) Temperature dependence of resistance under different in-plane magnetic fields, from 0 to 14 T in 1 T steps. The left inset shows the schematic illustration of the magnetic field and MoS_2 plane, and the right inset is a close-up view of the data near T_c. c) The B_{c2} normalized by B_p, as a function of the reduced temperature T/T_c, for different V_{BG}. Inset: The slope of the linear region as a function of V_{BG}. d) Schematic illustration of the Zeeman-like effective field B_{eff} at the K/K' valleys. Different colors of the energy bands represent different spin polarizations. Superconductivity resides at the topmost layer, and the remaining bottom layers are still in the intrinsic semiconducting state. The Zeeman effective fields of adjacent layers are in opposite directions; hence, it weakens if interlayer coupling is strong.

whereas the bottom layers remain in their intrinsic semiconducting states. In contrast, once a positive V_{BG} is switched on, electrons accumulate in the bottom layers. Consequently, the bottom layers become conducting and their coupling with the top superconducting layer enhances. As the direction of the Zeeman effective field B_{eff} is opposite in the K/K' valleys of the adjacent layers (Figure 3d), more interlayer coupling will lead to the weakening of B_{eff}, so does the Ising protection. Correspondingly, a negative back gate depletes the electrons in the bottom layers, cutting off the connection between bottom layers and the top superconducting layer. The effective Zeeman field is maximum without coupling from the bottom layers; hence, Ising protection is stronger.

It should be noted that due to the large electrical field of ionic gating (≈50 mV cm^{-1}), in-plane Rashba-type spin splitting is also expected in our system. The presence of Rashba-type spin splitting weakens the strength of Ising protection as it tends to align spins to the in-plane direction. However, the Rashba-type spin splitting is expected to be suppressed at the positive back gate because the electrical field generated by a positive V_{BG} weakens that of the top ionic liquid gate; hence, an enhanced Ising protection should be observed, which is contradictory to our measurements. This suggests that the effect of Rashba-type spin splitting is not crucial in our analysis. Other possibilities such as the electrical field-induced band structure modification are expected to exhibit a weak effect due to the relatively small carrier density even at the superconducting phase, which needs further investigation.

In summary, we fabricated high-quality h-BN/MoS_2/h-BN heterostructures, which show well-defined SdH oscillations. An effective mass of 0.6 m_e and threefold Landau-level degeneracy confirm that the oscillating electrons are mainly contributed by the Q/Q' valleys. In the titled magnetic field, the SdH oscillations remain unchanged as a function of the perpendicular field component, suggesting that the spin of the Q/Q' valley is strongly pinned to the out-of-plane direction; hence, Zeeman energy is not sensitive to the in-plane field component.

© 2019 WILEY-VCH Verlag GmbH & Co. KGaA, Weinheim

Superconductivity is induced at the surface of the unencapsulated MoS_2. The spins of Cooper pairs at the K/K' valleys are strongly locked to the out-of-plane direction, hence are protected from being realigned by the in-plane magnetic field, known as Ising protection. Due to this protection, T_c only decreases by $\approx$0.3 K in an in-plane field of $B = 14$ T. In addition, the strength of Ising protection can be effectively tuned by back gate. While this tuning effect is not understood well yet, we propose it could be the result of back gate-induced modification of the coupling between the top superconducting layer and bottom semiconducting layers, which leads to the change in the Zeeman effective field. It should be emphasized that the device structure presented in this work can be easily generalized to other systems. Recently, substantial progress has been made in fabricating wafer-scale TMDs[33] and other 2D semiconductors such as post-transition metal compounds (GaS, GaSe, etc.).[34] Our work provides a simple and reliable way to probe and tune the spin textures of few-layer 2D semiconductors, which will facilitate the wafer-scale applications of TMDs and post-transition metal compounds in spin- and valley-tronics.

Acknowledgements

The authors thank Joost Zoestbergen for technical support. Q.C. thanks the scholarship from The Ubbo Emmius Fund. J.Y. and Q.C. thank the Stichting voor Fundamenteel Onderzoek der Materie (FOM, FV157) and FlagERA iSpinText for financial support. J.Y. acknowledges funding from the European Research Council (consolidator Grant No. 648855, Ig-QPD).

Conflict of Interest

The authors declare no conflict of interest.

Keywords

few-layer MoS_2, ionic liquid gating, Ising superconductivity, Shubnikov–de Haas oscillations, spin polarization

Received: June 9, 2019
Revised: July 12, 2019
Published online: August 20, 2019

[1] I. Žutić, J. Fabian, S. Das Sarma, *Rev. Mod. Phys.* **2004**, *76*, 323.
[2] D. Jariwala, V. K. Sangwan, L. J. Lauhon, T. J. Marks, M. C. Hersam, *ACS Nano* **2014**, *8*, 1102.
[3] Q. H. Wang, K. Kalantar-Zadeh, A. Kis, J. N. Coleman, M. S. Strano, *Nat. Nanotechnol.* **2012**, *7*, 699.
[4] X. Xu, W. Yao, D. Xiao, T. F. Heinz, *Nat. Phys.* **2014**, *10*, 343.
[5] J. R. Schaibley, H. Yu, G. Clark, P. Rivera, J. S. Ross, K. L. Seyler, W. Yao, X. Xu, *Nat. Rev. Mater.* **2016**, *1*, 16055.
[6] R. Pisoni, Y. Lee, H. Overweg, M. Eich, P. Simonet, K. Watanabe, T. Taniguchi, R. Gorbachev, T. Ihn, K. Ensslin, *Nano Lett.* **2017**, *17*, 5008.
[7] J. Lin, T. Han, B. A. Piot, Z. Wu, S. Xu, G. Long, L. An, P. Cheung, P.-P. Zheng, P. Plochocka, X. Dai, D. K. Maude, F. Zhang, N. Wang, *Nano Lett.* **2019**, *19*, 1736.
[8] S. Larentis, H. C. P. Movva, B. Fallahazad, K. Kim, A. Behroozi, T. Taniguchi, K. Watanabe, S. K. Banerjee, E. Tutuc, *Phys. Rev. B* **2018**, *97*, 201407.
[9] R. Pisoni, A. Kormányos, M. Brooks, Z. Lei, P. Back, M. Eich, H. Overweg, Y. Lee, P. Rickhaus, K. Watanabe, T. Taniguchi, A. Imamoglu, G. Burkard, T. Ihn, K. Ensslin, *Phys. Rev. Lett.* **2018**, *121*, 247701.
[10] B. Fallahazad, H. C. P. Movva, K. Kim, S. Larentis, T. Taniguchi, K. Watanabe, S. K. Banerjee, E. Tutuc, *Phys. Rev. Lett.* **2016**, *116*, 086601.
[11] X. Cui, G.-H. Lee, Y. D. Kim, G. Arefe, P. Y. Huang, C.-H. Lee, D. A. Chenet, X. Zhang, L. Wang, F. Ye, F. Pizzocchero, B. S. Jessen, K. Watanabe, T. Taniguchi, D. A. Muller, T. Low, P. Kim, J. Hone, *Nat. Nanotechnol.* **2015**, *10*, 534.
[12] Z. Wu, S. Xu, H. Lu, A. Khamoshi, G.-B. Liu, T. Han, Y. Wu, J. Lin, G. Long, Y. He, Y. Cai, Y. Yao, F. Zhang, N. Wang, *Nat. Commun.* **2016**, *7*, 12955.
[13] J. T. Ye, Y. J. Zhang, R. Akashi, M. S. Bahramy, R. Arita, Y. Iwasa, *Science* **2012**, *338*, 1193.
[14] W. Shi, J. Ye, Y. Zhang, R. Suzuki, M. Yoshida, J. Miyazaki, N. Inoue, Y. Saito, Y. Iwasa, *Sci. Rep.* **2015**, *5*, 12534.
[15] S. Jo, D. Costanzo, H. Berger, A. F. Morpurgo, *Nano Lett.* **2015**, *15*, 1197.
[16] J. Lu, O. Zheliuk, Q. Chen, I. Leermakers, N. E. Hussey, U. Zeitler, J. Ye, *Proc. Natl. Acad. Sci. USA* **2018**, *115*, 3551.
[17] P. J. Zomer, M. H. D. Guimarães, J. C. Brant, N. Tombros, B. J. van Wees, *Appl. Phys. Lett.* **2014**, *105*, 013101.
[18] Q. Chen, J. Lu, L. Liang, O. Zheliuk, A. A. E. Yumin, J. Ye, *Adv. Mater.* **2018**, *30*, 1800399.
[19] J. T. Ye, S. Inoue, K. Kobayashi, Y. Kasahara, H. T. Yuan, H. Shimotani, Y. Iwasa, *Nat. Mater.* **2010**, *9*, 125.
[20] J. M. Lu, O. Zheliuk, I. Leermakers, N. F. Q. Yuan, U. Zeitler, K. T. Law, J. T. Ye, *Science* **2015**, *350*, 1353.
[21] Q. Chen, L. Liang, A. Ali El Yumin, J. Lu, O. Zheliuk, J. Ye, *Phys. Status Solidi B* **2017**, *254*, 1700181.
[22] B. W. H. Baugher, H. O. H. Churchill, Y. Yang, P. Jarillo-Herrero, *Nano Lett.* **2013**, *13*, 4212.
[23] B. Radisavljevic, A. Kis, *Nat. Mater.* **2013**, *12*, 815.
[24] J.-H. Chen, C. Jang, S. Xiao, M. Ishigami, M. S. Fuhrer, *Nat. Nanotechnol.* **2008**, *3*, 206.
[25] T. Ando, A. B. Fowler, F. Stern, *Rev. Mod. Phys.* **1982**, *54*, 437.
[26] S. Das Sarma, S. Adam, E. H. Hwang, E. Rossi, *Rev. Mod. Phys.* **2011**, *83*, 407.
[27] Q. H. Chen, J. M. Lu, L. Liang, O. Zheliuk, A. Ali, P. Sheng, J. T. Ye, *Phys. Rev. Lett.* **2017**, *119*, 147002.
[28] Y. Li, J. Ludwig, T. Low, A. Chernikov, X. Cui, G. Arefe, Y. D. Kim, A. M. van der Zande, A. Rigosi, H. M. Hill, S. H. Kim, J. Hone, Z. Li, D. Smirnov, T. F. Heinz, *Phys. Rev. Lett.* **2014**, *113*, 266804.
[29] A. Srivastava, M. Sidler, A. V. Allain, D. S. Lembke, A. Kis, A. Imamoğlu, *Nat. Phys.* **2015**, *11*, 141.
[30] D. MacNeill, C. Heikes, K. F. Mak, Z. Anderson, A. Kormányos, V. Zólyomi, J. Park, D. C. Ralph, *Phys. Rev. Lett.* **2015**, *114*, 037401.
[31] G. Aivazian, Z. Gong, A. M. Jones, R.-L. Chu, J. Yan, D. G. Mandrus, C. Zhang, D. Cobden, W. Yao, X. Xu, *Nat. Phys.* **2015**, *11*, 148.
[32] G.-B. Liu, W.-Y. Shan, Y. Yao, W. Yao, D. Xiao, *Phys. Rev. B* **2013**, *88*, 085433.
[33] K. Kang, S. Xie, L. Huang, Y. Han, P. Y. Huang, K. F. Mak, C.-J. Kim, D. Muller, J. Park, *Nature* **2015**, *520*, 656.
[34] B. J. Carey, J. Z. Ou, R. M. Clark, K. J. Berean, A. Zavabeti, A. S. R. Chesman, S. P. Russo, D. W. M. Lau, Z.-Q. Xu, Q. Bao, O. Kavehei, B. C. Gibson, M. D. Dickey, R. B. Kaner, T. Daeneke, K. Kalantar-Zadeh, *Nat. Commun.* **2017**, *8*, 14482.

© 2019 WILEY-VCH Verlag GmbH & Co. KGaA, Weinheim